On the synthesis of N-O bearing species in astrophysical ices-an infrared spectroscopic study using heavy-ion irradiation of solid N2:CO samples

A Bergantini, A De barros, Alicja Domaracka, H Rothard, P Boduch, E Da silveira

On the synthesis of N–O bearing species in astrophysical ices – an infrared spectroscopic study using heavy-ion irradiation of solid N_2:CO samples

A. Bergantini [1]<*>, A. L. F. de Barros [2], A. Domaracka,[3] H. Rothard,[3] P. Boduch[3] and E. F. da Silveira[4]

[1] *Department of Electronic Engineering, Centro Federal de Educação Tecnológica Celso Suckow da Fonseca, Av Maracanã 229, 20271-110 Rio de Janeiro, RJ, Brazil*

[2] *Department of Physics, Centro Federal de Educação Tecnológica Celso Suckow da Fonseca, Av Maracanã 229, 20271-110 Rio de Janeiro, RJ, Brazil*

[3] *Centre de Recherche sur les Ions, les Matériaux et la Photonique (CEA/CNRS/ENSICAEN/UNICAEN/Normandie Univ.), CIMAP-CIRIL-Ganil, Boulevard Henri Becquerel, CS 65133 14076, Cedex 5 Caen, France*

[4] *Department of Physics , Pontifícia Universidade Católica do Rio de Janeiro, Rua Marquês de São Vicente 225, 22451-900, Rio de Janeiro, RJ, Brazil*

ABSTRACT

The interstellar chemistry of nitrogen is considerably less understood than the chemistry of other common elements, such as carbon and oxygen. Even though a relatively large number of species containing nitrogen atoms have already been detected in the interstellar medium, only six of them bear a nitrogen–oxygen (N–O) bond. Some astrophysical and primeval Earth models suggest that N–O species, such as hydroxylamine (NH_2OH), are potential precursors of prebiotic amino acids, and even peptides. In this work, we have analyzed an apolar ice mixture of N_2:CO of astrophysical interest to investigate possible formation mechanisms of N–O bearing molecules due to processing of the sample by $^{64}Ni^{24+}$ 538 MeV ions (8.4 MeV/u) at 14 K. The results show the formation of simple nitrogen oxides ($N_{1-2}O_y$), but no CN–O species of any kind. We have also determined the formation cross-sections of some of the products, as well as the destruction cross-sections of precursors and products. The results presented here are discussed in light of our previous work on the processing of a NH_3:CO ice mixture, which have found no N–O bearing molecules at all.

Key words: astrochemistry – molecular data – techniques: spectroscopic – methods: laboratory: molecular – interplanetary medium.

1 INTRODUCTION

According to the *Cologne Database for Molecular Spectroscopy* (Müller et al. 2001), as of late 2021, at least 210 chemical species have been detected in different regions of the interstellar medium (ISM) and in circumstellar shells. Among them, only six species bearing an N–O (nitrogen–oxygen) bond have been found so far. They are nitric oxide (NO), nitrous oxide (N_2O), nitroxyl (HNO), nitrous acid (HONO), fulminic acid (HCNO), and hydroxylamine (NH_2OH) (Fig. 1). What makes this matter remarkable is the fact that oxygen and nitrogen are, respectively, the second and fourth most abundant chemical elements in the visible Universe (not accounting for unreactive He and Ne) (Cameron 1973). Even though the availability of each element may differ considerably throughout a galaxy (Meyer, Jura & Cardelli 1998), it is safe to assume that both N and O are readily available in any given ISM object. Therefore, the reasons why so few species bearing an N–O bond have been detected in astrophysical objects so far are worthy of further investigation. This is particularly relevant because nitrogen oxides are believed to be the main precursors of hydroxylamine (NH_2OH), a molecule that plays a crucial role on the interstellar formation routes of amino acids according to many astrophysical models (Charnley et al. 2001; Blagojevic, Petrie & Bohme 2003; Rivilla et al. 2020), hydroxylamine may even be involved in reaction pathways of peptide formation in Earth's primeval sea (Sakurai & Yanagawa 1984).

A previous investigation by de Barros et al. (2020) on the processing of an CO:NH_3 ice mixture of astrophysical interest showed no evidence of formation of molecules containing both N and O. Despite the potential large availability of oxygen and nitrogen atoms and radicals within the sample CO:NH_3, no species with general formulas $H_xC_yN_zO_k$, $C_yN_zO_k$, or N_zO_k (with x, y, z, $k \geq 1$) were observed. This result prompted the research presented here on the processing of a N_2:CO ice mixture under the same experimental conditions as the work of de Barros et al. Note that, even though interstellar ice grains are commonly dominated by polar species, such as H_2O, alcohols, and nitriles, some Solar system bodies and interstellar ice mantles are thought to have regions deficient in H_2O ice and rich in apolar species, such as N_2, O_2, and CO (see Hudson 2018 and references therein). These species are potential precursors of interstellar N–O bearing molecules. Therefore, this work presents the processing (by heavy and swift ions) of a nitrogen- rich N_2:CO ice mixture, intended to investigate the mechanisms behind the synthesis of N–O bond bearing species in interstellar and circumstellar objects. The experiment was performed in a high-vacuum chamber, and the sample was irradiated by $^{64}Ni^{24+}$ ions at 538 MeV. The chemical evolution of the ice sample was probed *in situ* by Fourier Transform Infrared (FTIR) spectroscopy. The data analysis employed supplementary techniques such as *peak*

* E-mail: alexandre.souza@cefet-rj.br

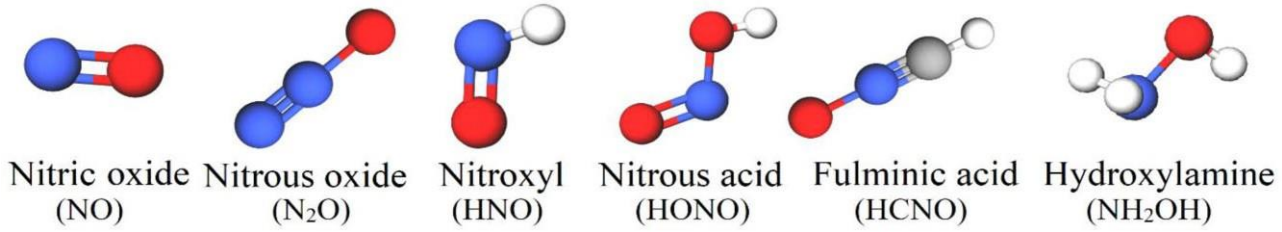

Figure 1. Among the more than 210 chemical species identified in the interstellar medium (Müller et al. 2001) so far, were detected only six species bearing an N–O bond.

fitting and *noise attenuation* using *Locally Weighted Scatterplot Smoothing* (LOWESS) and *Savitzky-Golay* (S-G) filter. Confirming previous research, the results presented here suggest that the relative absence of N–O bearing species in interstellar objects may be due to unfavourable formation mechanisms rather than to detection constraints from space or Earth-based telescopes (McGonagle 1995; Ponciano et al. 2008; Pulliam, McGuire & Remijan 2012; Coutens et al. 2019). The results show that only five molecular species containing an N–O bond were found (including two species that have also been detected in the ISM), but none of the reported species bear at least one carbon atom in addition to the N–O bond. Additionally, our results support the suggestion that observational astronomers should look for the nitrogen oxides NO_2, N_2O_3, and N_2O_4 towards astrophysical objects where NO and N_2O have already been detected.

2 METHODS

The experiments were carried out in a high vacuum chamber at the IRRadiation SUD (IRRSUD) beamline of the French National Heavy Ion Accelerator (GANIL), using the CASIMIR set-up of CIMAP-CIRIL (Centre de recherche sur les Ions, Matériaux et la Photonique). Details on the operation of GANIL and IRRSUD beamline were described by Duarte et al. (2009) and de Barros et al. (2011). The mixture investigated in this study was prepared in a separate chamber by admitting 18 mbar of N_2 gas (99.995 per cent purity, Messer Griesheim) and 2 mbar of CO gas (99.97 per cent purity, Linde Gas). Then the mixture was deposited on a CsI substrate by a capillary injection tube held approximately 10 mm away from the substrate. The substrate is attached to a cold finger cooled to 14 K by a closed-cycle helium cryostat. The experiment takes place inside a high-vacuum chamber (base pressure of low-10^{-8} mbar) connected to the ion IRRSUD beamline. The ice sample was probed by a Nicolet Magna 550 Fourier Transform Infrared Spectrometer running in absorption mode, with the beam impinging perpendicularly to the surface of the sample. Each IR spectrum was acquired by 256 scans in the 5000–600 cm^{-1} (2–16.7 μm) region, at 4 cm^{-1} of resolution. The initial column density of each species in the unirradiated sample was calculated using the Lambert–Beer relationship and they were based on the fundamental mode of CO at 2139 cm^{-1} and in the infrared forbidden fundamental mode of N_2 at 2327.7 cm^{-1}. The infrared band strengths (*A-Values*) used in the column density calculation were $(1.12 \pm 0.05) \times 10^{-17}$ cm molecule^{-1} (Bouilloud et al. 2015) and $(2.9 \pm 0.5) \times 10^{-22}$ cm molecule^{-1} (Bernstein & Sandford 1999), for CO and N_2, respectively, which yielded an initial N_2/CO ratio of (15 ± 3) to 1. The initial sample thickness of (6.5 ± 0.5) μm was calculated using $L = \frac{N_0 M}{\rho N_A}$, where N_0 is the initial column density of each species [cm^{-2}], M is the molar mass [u], ρ is density [g cm^{-3}], and N_A is the Avogadro's number. The density used for N_2 and CO were 1.2071 g cm^{-3} and 0.8 g cm^{-3}, respectively (Bernstein & Sandford 1999; Bouilloud et al. 2015). The sample was irradiated by a 538 MeV (8.4 MeV/u), $^{64}Ni^{24+}$ ion beam for 190 min at an average flux of 1.16 10^9 ions per second. The total energy deposited of (20 2) eV molecule^{-1} was estimated using the SRIM package (Ziegler, Ziegler & Biersack 2010). Signal processing (i.e. smoothing and filtering) was performed using OriginPro 2018 software and peak fitting was performed using GRAMS/AI software (version 9.2).

3 RESULTS

3.1 Infrared spectroscopy

The chemical evolution of the sample was monitored by FTIR spectroscopy before and after each step of irradiation. A broad view of the spectra as a function of fluence can be seen in Fig. 2, where fluence increases from bottom to top. Features seen at 4275, 3750, 1234, 1200, and 804 cm^{-1} in Fig. 2 are an anomalous dispersion effect related to resonant Mie (RMie) scattering (Bassan et al. 2010; Miljković, Bird & Diem 2012), and they do not interfere with the rest of the spectrum.

Since N_2 is normally inactive in the IR region, the spectrum at the beginning of the experiment is dominated by vibrational modes of CO and its isotopologues, plus a very small amount of CO_2 impurity (identified by small bands at 3707 and at 2346 cm^{-1}). Nevertheless, it is known that the forbidden N_2 fundamental vibration near 2328 cm^{-1} may become active in infrared in solid samples due to interactions with neighboring species, such as CO or H_2O, which can break the electrostatic symmetry of N_2 (Bernstein & Sandford 1999; de Barros et al. 2015). Interestingly, upon first inspection, the 2328 cm^{-1} band, belonging to the fundamental mode of N_2, seemed absent. However, it became visible once the data was treated using either LOWES smoothing (Cleveland 1979) or S-G filter (Bromba & Ziegler 1981), as seen in Fig. 3. As another example, in addition to the fundamental of N_2, Fig. 3 also shows the 2100–1950 cm^{-1} region at 2 10^{12} cm^{-2} of fluence, where additional bands were also confirmed using LOWESS. Note the extremely low absorbance values in both Fig. 3 insets, which is the main reason why smoothing and filtering techniques had to be employed.

Detailed IR features found across all the fluences of the experiment can be seen in Fig. 4, where the spectrum was divided in regions of interest. Moreover, Fig. 4 shows the IR bands that were identified without additional data treatment (i.e. without smoothing or peak fitting). The IR features shown in Fig. 4 are listed in Table 1.

Some remarks regarding Fig. 4: the drop in signal at 4275 cm^{-1} in Fig. 4(b) is due to RMie scattering; in Fig. 4(c), the shoulder that appears at 3703 cm^{-1} in higher fluences is assigned to conformational CO_2 (Duarte et al. 2021); the very weak band at 2910 cm^{-1} (Fig. 4d) is attributed to nitrous oxide (N_2O); Fig. 4(h) shows a narrow band at 1875 cm^{-1}, which, according to the literature, could be the ν_1 mode

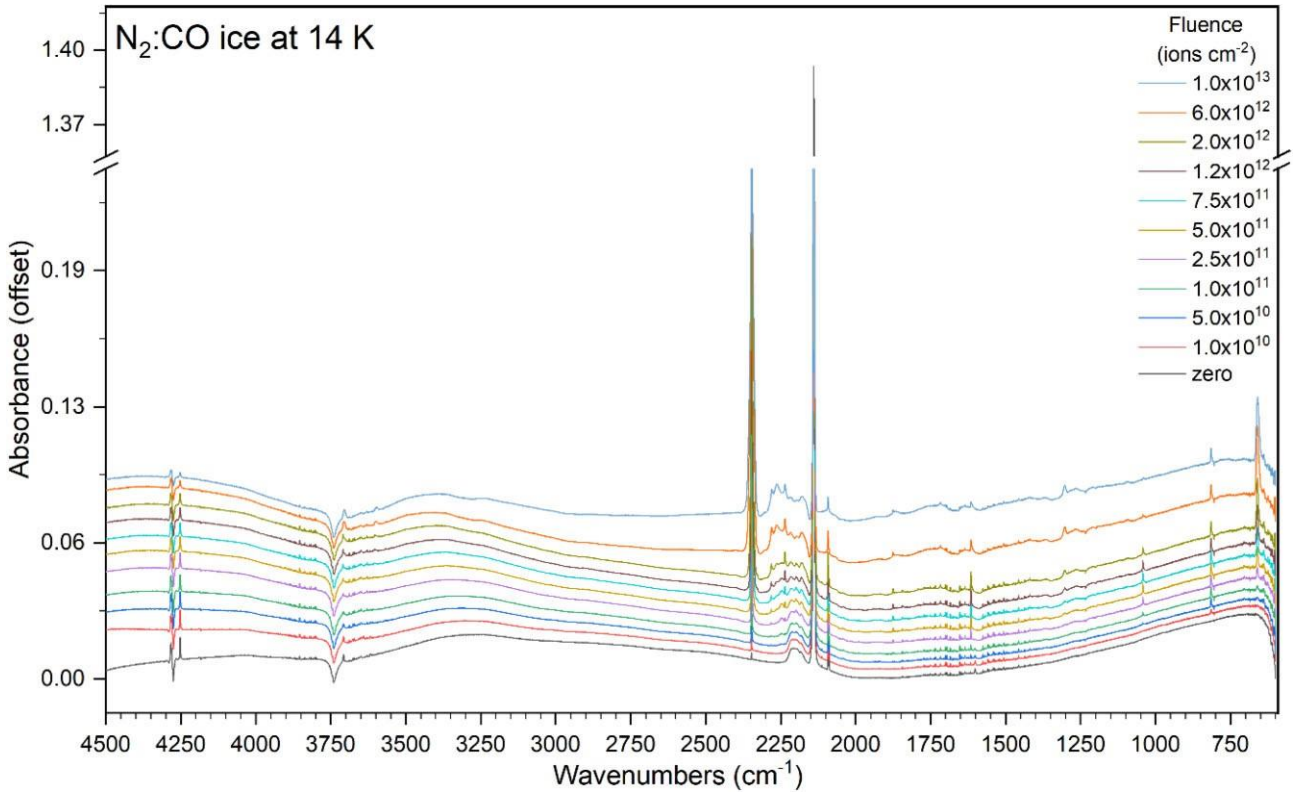

Figure 2. Evolution of the N_2: CO spectra over the range of fluences. Fluence increases from bottom to top, with the lowermost spectrum corresponding to the unirradiated sample.

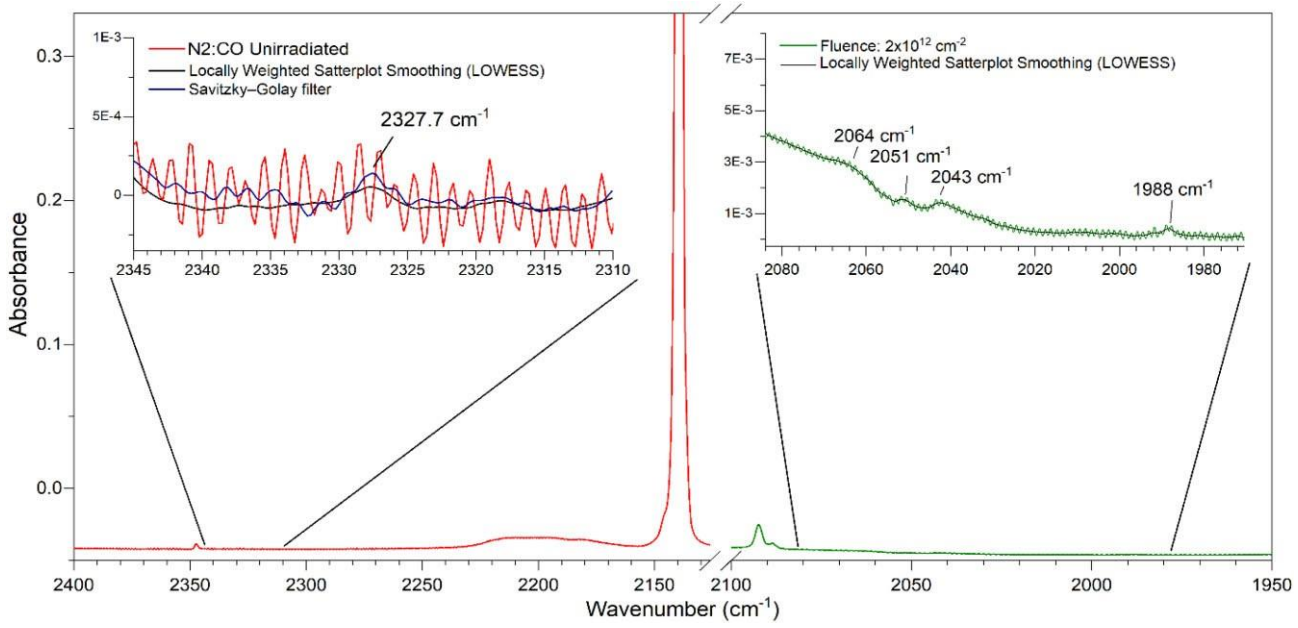

Figure 3. Data smoothing was used to evince signals which would be interpreted as noise otherwise. Left-hand side (red): Unirradiated spectrum of the N_2:CO sample. The inset shows the infrared forbidden fundamental mode of solid N_2, made evident by two separate techniques, namely, Locally Weighted Scatterplot Smoothing (LOWESS) and Savitzky–Golay (S–G) filter. Right-hand side (green): Spectrum at fluence of 2×10^{12} cm^{-2}. The inset exemplifies the use of filters to evince IR bands. Note the extremely low absorbance of the IR signal in both insets. The result is achieved by fitting successive sub-sets of adjacent data points with a low-degree polynomial by the method of linear least squares.

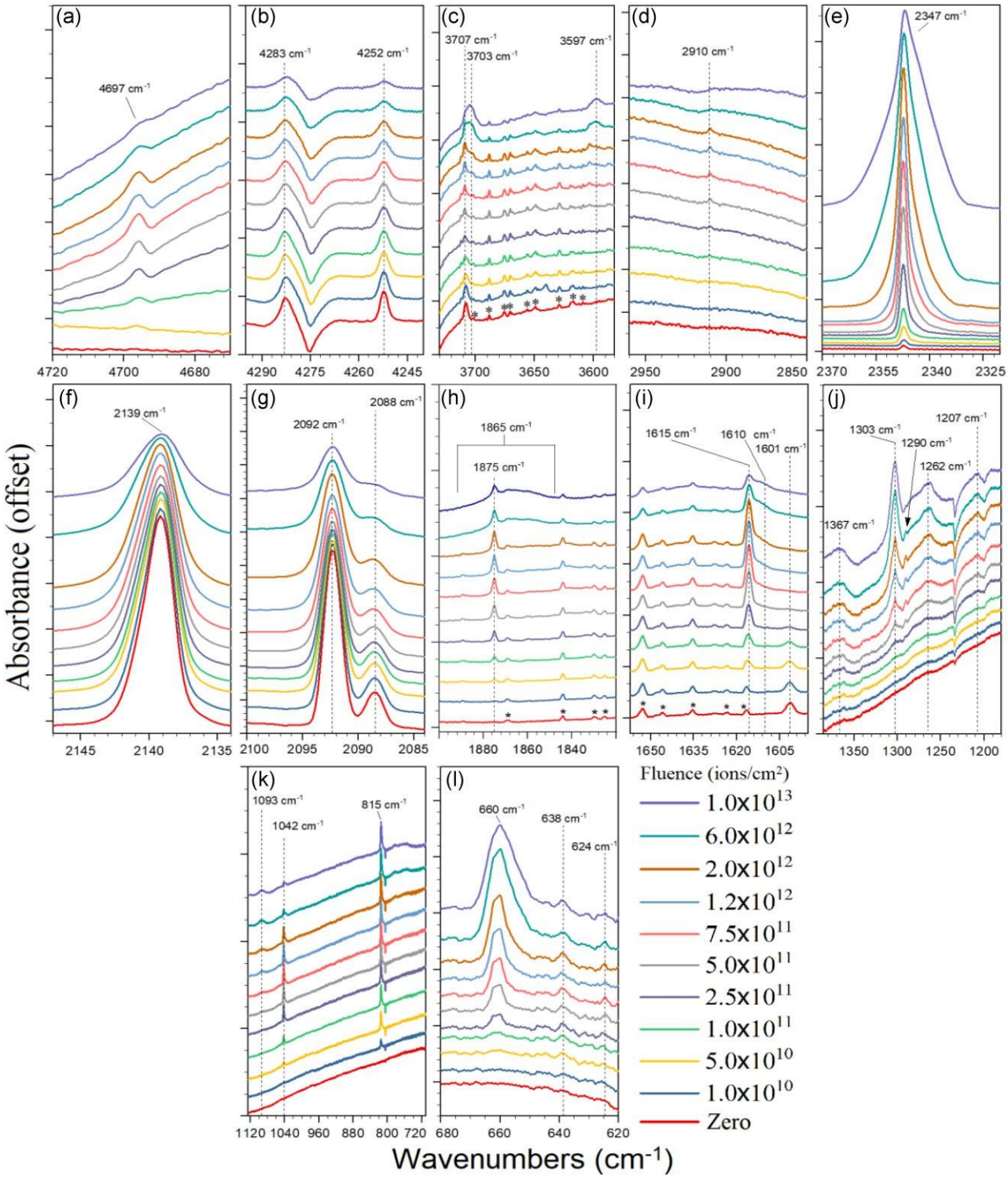

Figure 4. Detailed view of the main bands detected throughout the experiment. Fluence increases from bottom to top. Spurious atmospheric gas in the IR beam line of sight.

of NO monomer and/or the Fermi resonance of CO_3 (Jamieson et al. 2005). Fig. 4(h) also shows a wider band centred at 1865 cm^{-1}, which is assigned to the ν_1 mode of cis-$(NO)_2$ (Fedoseev et al. 2012; Hudson 2018); the 1615 cm^{-1} band seen in Fig. 4(i) is frequently reported as belonging to nitrogen dioxide (NO_2) (Hudson 2018), even though Fedoseev et al. (2012) assigns it to dinitrogen trioxide (N_2O_3). In the same figure, the small shoulder at 1610 cm^{-1}, which is only seen towards the end of the experiment, is most likely a shift of the 1615 cm^{-1} band due to changes in density and temperature of the ice**.** Indeed, this band has not been reported for similar experiments. The 1601 cm^{-1} band has been reported in the literature as azide radical ($^{15}N_3$) (Tian, Facelli & Michl 1988; Jamieson & Kaiser 2007).

Table 1. Position and assignment of the vibrational bands detected by FTIR spectroscopy before and after the processing of the sample by heavy and swift ions.

Position (cm^{-1})					
Before irradiation	After irradiation	Literature reference	Assignment	Obs.	References
	4697	4698	CO_2	$2\nu_3$	[1]
4283	–	4283	CO	–	[1]
4252	–	4252	CO	Comb.	[2]
3707 ζ	3707	3708	CO_2	–	[2]
	3703	–	CO_2	Conformer	[3]
	3597	3600	CO_2	$2\nu_2+\nu_3$	[2]
	2910	2908	NO_2	$\nu_1 + \nu_3$	[4]
2347 ζ	2347	2343	CO_2	ν_3	[2]
2327	–	2328	N_2	ν_1	[5]
2139	–	2139	CO	Str.	[2]
2092	–	2093	^{13}CO	Str.	[2]
2088	–	2089	$C^{18}O$	–	[1]
	2064	2066	Unknown	–	[1]
	2051	2051	Unknown	–	[1]
	2043	2043	CN	–	[1]
	1988	1988	C_2O	–	[1]
	1934	1934	OCN	–	[1]
	1923	1924	Unknown	–	[1]
	1875	1875	NO	ν_1, monomer	[6]; [7]
	–	1876	CO_3	Fermi resonance	[8]
	1865	1864	NO	ν_1, cis-$(NO)_2$	[4]; [7]
	–	1867	N_2O_3	–	[6]
	1615	1615	NO_2	ν_3	[6]; [9]
1601	–	–	Noise?	–	–
	1367	–	Unknown	–	–
	1303	1303	N_2O_3	ν_3	[6]; [10]
	1290	1290	N_2O_4	ν_1	[6]
	1262	1262	N_2O_4	Stable planar	[6];[10]
	1093	1091	Unknown	–	[1]
	1042	1043	O_3	ν_3	[1]; [8]; [11]
	815	–	Unknown	–	–
	660	660	CO_2	ν_2	[2]
	638	638	$^{13}CO_2$	ν_2	[12]
	624	–	Unknown	–	–

References: [1] Sicilia et al. (2012); [2] Bouilloud et al. (2015); [3] Duarte et al. (2021); [4] Hudson (2018); [5] Bernstein and Sandford (1999); [6] Fateley et al. (1959); [7] Krim (1998); [8] Jamieson et al. (2005); [9] Varetti and Pimentel (1971); [10] Fulvio et al. (2019); [11] Bennett, Jamieson & Kaiser (2009); [12] Bennett et al. (2004)

However, since this signal is seen even in the unirradiated sample, it is also possible that the 1601 cm^{-1} band is atmospheric noise which is being hidden by the 1610 cm^{-1} band as it becomes more intense at higher fluences. Asterisks in Fig. 4(c), (h), and (i) are indicating spurious atmospheric gas in the IR beam line of sight. The 1367 cm^{-1} band in Fig. 4(j) is unknown; the 1303 cm^{-1} band in Fig. 4(j) is assigned to N_2O_3 (Fateley et al. 1959), the 1290 cm^{-1} and the 1262 cm^{-1} bands are assigned to dinitrogen tetroxide (N_2O_4) (Fateley et al. 1959). Signals at 1233 cm^{-1} and at 1207 cm^{-1} are believed to be RMie scattering. The assignment of the weak band at 1093 cm^{-1} (Fig. 4k) is unknown, even though it has also been reported by Sicilia et al. (2012). It is undecided if the 815 cm^{-1} peak, which has not been reported in the literature for similar systems, is an actual molecular vibration or just an effect of RMie scattering. Similarly, the 624 cm^{-1} peak in Fig. 4(l) may merely be noise, since we have not found reports of this band for similar experiments. Finally, the 1934 cm^{-1} band (cyanate ion, OCN^-, Table 1) was not included in Fig. 4 because of its low intensity, which makes it difficult to identify without LOWES smoothing. For this reason, the spectrum of the 2075–1900 cm^{-1} region is shown only in the *Supporting Information*.

The IR bands found between 2320 and 2155 cm^{-1} are much more difficult to resolve. Therefore, peak fitting was used to identify both parent and daughter bands in this region, as shown in Fig. 5.

The possible shortcomings related to the use of peak fitting in this type of research have been discussed by de Barros et al. (2020), and they have been taken into account is this work. Therefore, even though results from peak fitting should be taken cautiously, the IR bands unveiled in Fig. 5, and listed on Table 2, are presented with great confidence. It is worth to mention that, as discussed by e.g. de Barros et al. (2020), it is usually easier to fit any given region by adding several peaks to the fit until the sum of peaks matches the actual spectrum; however, the experience shows that this approach is, in most cases, just a mathematical fluke. Therefore, the fit presented here was done by adding the fewest possible number of peaks which would still result in a good fit, which was evaluated based on the residual value of the sum of peaks. Also, a set of fitted peaks should work as an adequate starting point for the fitting of that same region at the next (higher) fluence. To illustrate the results, three phases of the experiment were chosen: the unirradiated sample (Fig. 5a), an intermediary fluence (Fig. 5b), and the highest fluence of the experiment (Fig. 5c). These results are discussed next.

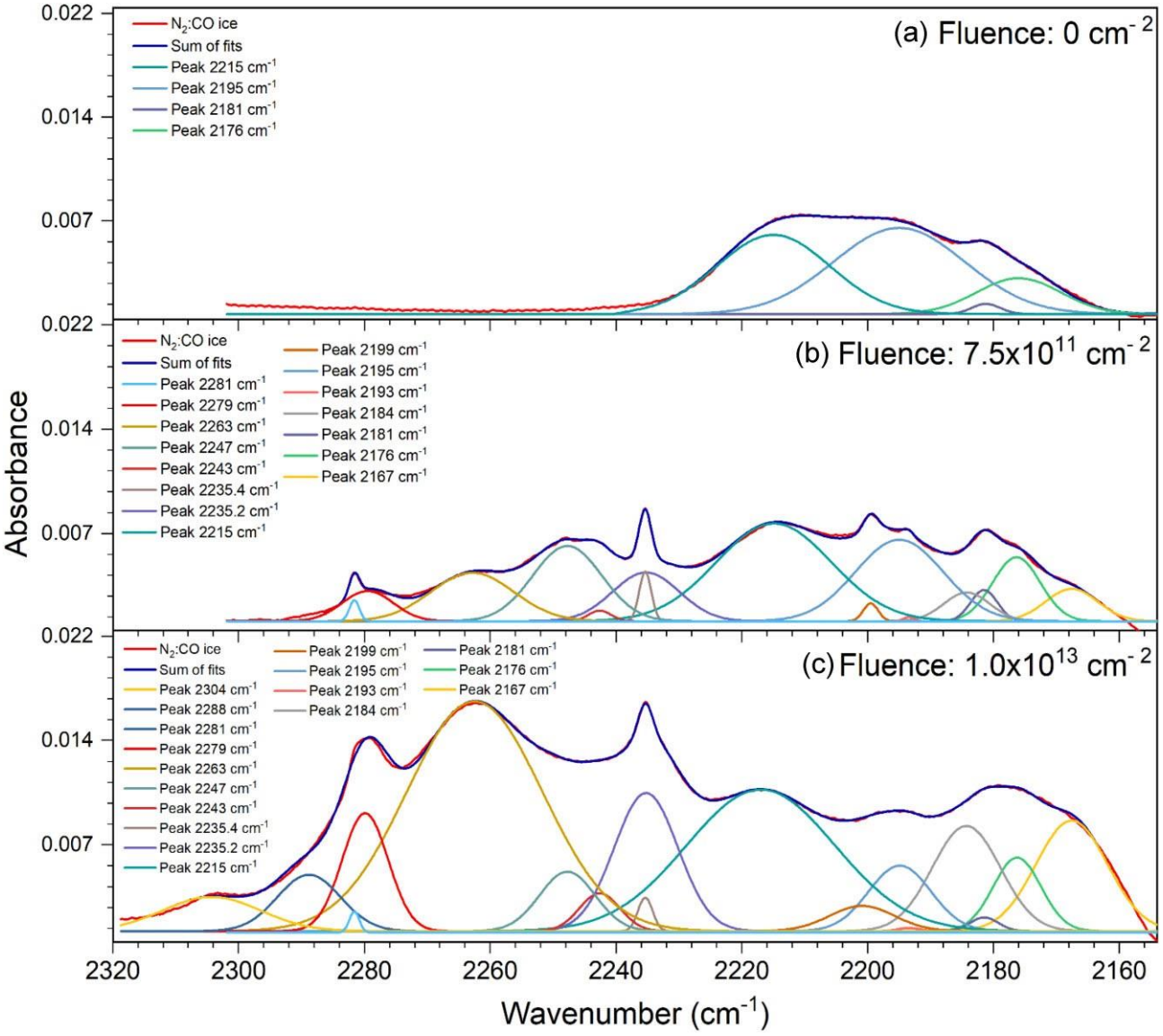

Figure 5. Data fitting of the 2300–2155 cm^{-1} region. The red line is the original data, the blue line is the sum of fits. Each peak is identified by its central position. (a) unirradiated sample, (b) intermediary dose, and (c) highest dose of irradiation.

The wide IR signal seen in Fig. 5(a) can be fitted by not less than four peaks. Because the spectrum seen in Fig. 5(a) is the spectrum of the unirradiated sample, these peaks cannot stem from irradiation products. Moreover, even though these bands are not commonly associated with CO in frozen mixtures, Jamieson, Mebel & Kaiser (2006) and Duarte et al. (2010) have also observed these vibrations in neat CO ices at 14 K in UHV conditions. The main difference between our and previous studies is the fact that we have fitted four peaks in the large band centered at around 2208 cm^{-1}. Fig. 5(b) shows the spectrum at a fluence of 7.5 $\times 10^{11}$ cm^{-2}, reached after 50 min of irradiation by 538 MeV $^{64}Ni^{24+}$ ions. The absorbance signal is broad and unresolved, therefore, only a few bands can be directly inferred. The region seen in Fig. 5(b) can be satisfactorily fitted by not less than fifteen peaks (see Table 2). In this fit are also included the four bands observed in the spectrum of the unirradiated sample (Fig. 5a). The spectrum at the highest dose, reached after 190 min of irradiation, is seen in Fig. 5(c). The data can be well fitted by not less than seventeen peaks (see Table 2). Among them are the fifteen peaks detected at lower fluences, plus two new peaks found at 2304 and 2288 cm^{-1}. Table 2 shows that there is an excellent agreement between the fits made at different fluences, which indicates that the qualitative results are plausible. On the other hand, when so many bands are being fitted simultaneously, the same cannot be said of the quantitative results, given the fact that even small tweaks in the fitting parameters may increase the area under the curve of any given band, while decreasing the area of an adjacent band, for example. The exceptions are the signals corresponding to CO_2 (at 2347 cm^{-1}), $^{13}CO_2$ (at 2281 cm^{-1}), C_3O (at 2263 cm^{-1}), and N_2O (at 2235 cm^{-1}), which are distinct enough to be included in the formation cross-section calculations (see Section 3.2). Next, we discuss some of the findings from the fittings shown in Fig. 5(b) and (c).

To our knowledge, no assignments for the 2304, 2288, 2279, 2263, 2235.2, and 2199 cm^{-1} bands (seen in Fig. 5b and c, also listed in Table 2) have not been published yet, most likely because they are undetectable without peak fitting. Even though the 2304, 2263, and 2199 cm^{-1} bands have also been reported by Sicilia et al. (2012)

Table 2. Positions of infrared vibrations for parent and daughter species detected within the 2320 cm^{-1} and 2155 cm^{-1} region using data fitting as shown in Fig. 5.

Zero	Fluence 7.5×10^{11} cm^{-2}	Fluence 1.0×10^{13} cm^{-2}	Assignment	Reference
–	–	2304 cm^{-1}	unknown	[1]
–	–	2288 cm^{-1}	unknown	–
–	2281 cm^{-1}	2281 cm^{-1}	$^{13}CO2$	[2]
–	2279 cm^{-1}	2279 cm^{-1}	unknown	–
–	2263 cm^{-1}	2263 cm^{-1}	C_3O^a	[3]
–	2247 cm^{-1}	2247 cm^{-1}	C ^{3}O	[1], [3]
–	2243 cm^{-1}	2243 cm^{-1}	N_2O	[4]
–	2235.4 cm^{-1}	2235.4 cm^{-1}	N_2O	[5]
–	2235.2 cm^{-1}	2235.2 cm^{-1}	unknown	–
2215 cm^{-1}	2215 cm^{-1}	2215 cm^{-1}	CO ($\upsilon_1 + \nu_L$)	[6]
–	2199 cm^{-1}	2199 cm^{-1}	unknown	[1]
2195 cm^{-1}	2195 cm^{-1}	2195 cm^{-1}	CO ($\upsilon_1 + \nu_L$)	[6]
–	2193 cm^{-1}	2193 cm^{-1}	C_3O_2	[1]
–	2184 cm^{-1}	2184 cm^{-1}	C_7O_2	[1]
2181 cm^{-1}	2181 cm^{-1}	2181 cm^{-1}	CO ($\upsilon_1 + \nu_L$)	[6]
2176 cm^{-1}	2176 cm^{-1}	2176 cm^{-1}	CO ($\upsilon_1 + \nu_L$)	[6]
–	2167 cm^{-1}	2167 cm^{-1}	OCN^-	[4]

References: [1] Sicilia et al. (2012); [2] Bouilloud et al. (2015); [3] Jamieson et al. (2006); [4] Ciaravella et al. (2019); [5] Fedoseev et al. (2012); [6] Jamieson et al. (2006). [a] The IR position of this band is a result of density functional theory calculation.

after processing similar N_2:CO mixtures by 200 keV protons, they were reported as unknown bands. Moreover, according to Socrates (1994), at room temperature, the 2300 cm^{-1} region of the IR spectrum contains stretching modes of cyanates and of species containing the –N⊆N, =C=N, –N=C=O, and –N=N=N groups, which, unfortunately cannot be confirmed at this point in our experiments. Among the other bands found in Fig. 5 and listed in Table 2, the only bands possibly bearing an N–O bond are the 2243 and 2235 cm^{-1} (both belonging to N_2O). Interestingly, the data fitting indicates that the 2235 cm^{-1} region is in fact composed of two peaks, one at 2235.4 and another 2235.2 cm^{-1}, respectively. To the best of our knowledge, there are no previous reports of this fact for similar experiments.

3.2 Physical parameters – cross-section calculations

Some physiochemical parameters, relevant to astrochemical models, have been calculated using the methodology described by de Barros et al. (2011, 2020). Fig. 6 shows how the column density of parent species CO and ^{13}CO evolve as a function of fluence. Using equation (1), and assuming a negligible variation of the band-strengths with fluence, the destruction cross-section dependence on fluence can be obtained by

$$N = N_0\ e^{-\sigma_d F}, \quad (1)$$

where N_0 is the initial column density of each species in the non-irradiated ice, σ_d is their destruction cross-sections, and F is fluence.

The evolution of the column density of each product can be modelled by equation (2) (de Barros et al. 2011; Mejía et al. 2013):

$$N_i(F) \approx N_0 \left(\frac{\sigma_{f,i}}{\sigma_d - \sigma_{d,i}}\right)[(e^{-\sigma_{d,i}F}) - (e^{-\sigma_d F})]. \quad (2)$$

Here, N_i (F) is the column density of the product i at fluence F, N_0 is the initial column density of the parent species, $\sigma_{f,i}$ and $\sigma_{d,i}$ are, respectively, formation and destruction cross-sections of species i, extracted by the $\frac{N_i(F)}{N_0}$ ratio as a function of fluence. In Fig. 7, the

Table 3 lists the parameters used to estimate the column densities of the parent and daughter species, as well as their calculated formation and destruction cross-sections.

4 DISCUSSION AND ASTROPHYSICAL IMPLICATIONS

According to reference infrared bands from the literature, the species bearing an N–O bond detected upon the processing of the N_2:CO sample at 14 K in this study are the nitrogen oxides NO (nitric oxide), N_2O (nitrous oxide), NO_2 (nitrogentab dioxide), N_2O_3 (dinitrogen trioxide), and N_2O_4 (dinitrogen tetroxide). Since our sample was nitrogen rich, it is conceivable that nitrogen molecular ions (N_2^+) are among the primary radiation products. The neutralization of N_2^+ can regenerate N_2 and even yield atomic nitrogen if the event is sufficiently energetic. The oxidation of nitrogen will yield NO, NO_2, plus potential N_xO_y isomers (Hudson 2018), some of which may be synthesized as *cis*- and *trans*-N_2O_2, asymmetric and symmetric N_2O_3, N_2O_4 and iso-N_2O_4, and so on. However, the data obtained in this study is not enough to address assignments to specific N_xO_y isomers. The most common charge-neutral nitrogen oxides detected in laboratory simulations are NO_x ($1 \leq x \leq 3$), N_2O_y ($1 \leq y \leq 5$), and N_4O_z ($z = 1, 6$), but so far, among all nitrogen oxides, only NO and N_2O have been detected towards ISM objects (Liszt & Turner 1978; Ziurys et al. 1994). Therefore, even though it is conceivable that larger nitrogen oxides ($N_{x>2}O_y$) and CN–O bearing species (i.e. species containing at least one N–O bond and one carbon) could be readily synthesized upon the energetic processing of N_2:CO ices (Sicilia et al. 2012; this work), the evidence suggests that such species are either lacking, or, at the very least, their yield too low to be detect by infrared spectroscopy in such systems. The same seems to apply to HCN–O bearing species (*i.e.* species containing at least one N–O bond, one hydrogen, and one carbon), which were not detected in our previous investigation on the processing of CO:NH_3 ices (de Barros et al. 2020). In fact, de Barros et al. (2020) have not detected any molecule containing both nitrogen and oxygen, bonded, or otherwise.

Other processes concerning the interstellar chemistry of nitrogen have been presented elsewhere. For example, Minissale et al. (2014) investigated routes where nitric oxide (NO) was the main precursor of larger interstellar nitrogen oxides. In their experiment, NO + O_{1-3} and NO + N beams where adsorbed into H_2O and ^{13}CO matrices, resulting in the formation of NO_2, N_2O, N_2O_4 (which were also detected in this work), and $ONNO_2$ (not found in this work). However, no CN–O or HCN–O bearing species were detected by *Minissale* and co-workers. In a similar experiment, Congiu et al. (2012) reported, *via* mass-spectrometry, the formation of hydroxylamine (NH_2OH) upon the hydrogenation of NO under dense cloud conditions. Fedoseev et al. (2016) investigated the nitrogen-carbon chemistry in NO/(H, CO, H_2CO, and CH_3OH) ices. They also observed the formation of the N–O bearing molecule hydroxylamine (NH_2OH) via hydrogenation of NO, and formation of the N–C bearing species isocyanic acid (HNCO), formamide (NH_2CHO), and cyanate ion (OCN^-) upon UV processing of the samples (note that these species do not bear an N–O bond). Therefore, our findings are in good agreement with studies in which the irradiation of nitrogen oxides (or similar species) was driving the main chemical changes. However, other processes, such as O-, C-, N-, and H-addition to nitrogen oxides,

solid lines correspond to the fitting using equation (2).

may enable additional mechanisms which were not considered in this work. As an example, the N–O bearing species dinitrogen trioxide ($ONNO_2$) and hydroxylamine (NH_2OH) were detected in hydrogen-addition experiments (Congiu et al. 2012; Fedoseev et al. 2016) but not in irradiation-driven experiments (e.g. Sicilia et al. 2012;

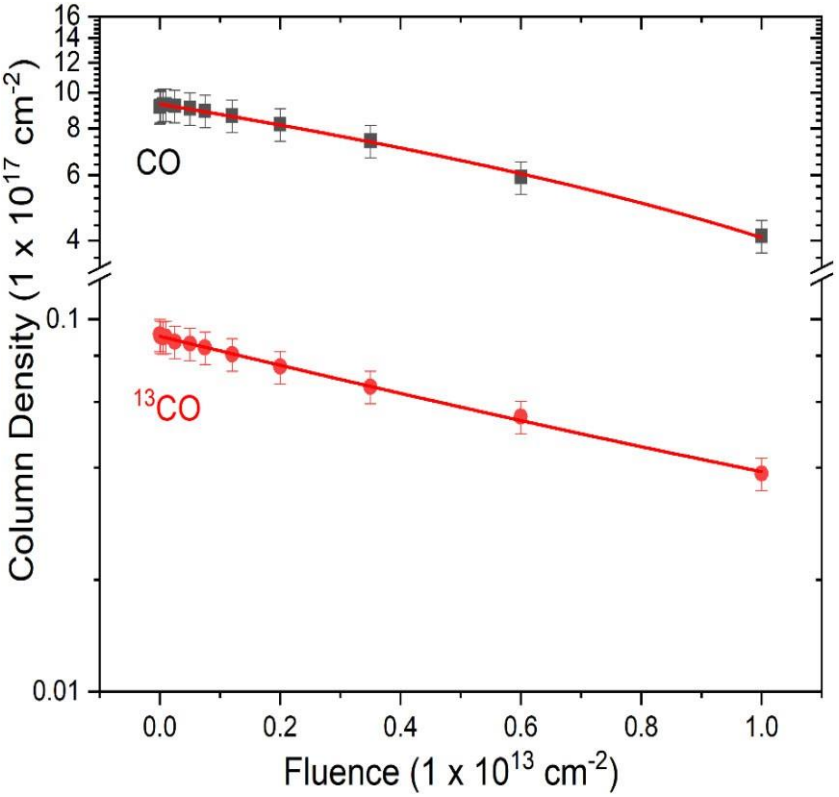

Figure 6. Column-density evolution of parent species CO and ^{13}CO with fluence. Solid lines are the fitting results obtained using equation (1).

this work). Conversely, one could argue that laboratory constraints are rather different than those of the interstellar medium, especially regarding chemical abundances of species found in analogue ices. In this respect, the absence of water in the astrophysical ice simulated in this work (and in the work of de Barros et al.) is the major discrepancy if compared to most ISM objects. However, as proposed by Bergantini, Maksyutenko & Kaiser (2017), and later demonstrated by Bergantini et al. (2018a), water, despite being the most abundant ice in the Universe, does not necessarily play the main role as precursor of every complex molecule detected in the ISM, especially when the polar/apolar nature of the ice is taken into account, since the reaction mechanisms involved may be totally different in each case. Therefore, the results presented here can be considered representative of irradiation-driven processes that may take place in real astrophysical objects, especially in regions dominated by apolar ices, and they suggest that the synthesis of H_mC_nN–O, C_nN–O, and $N_{x>2}O_y$ species is very unfavorable. Clearly, this assumption must be aided by computational models and by supplementary experiments to be considered definitively true.

Consequently, considering the limitations of infrared spectroscopy in discriminating the signal of molecules that share similar functional groups, and the limitations of mass-spectrometry in separating the signal from isomers (i.e. species with identical molecular formulas and monoisotopic mass), even when isotopic substitution and selective photoionization is employed (e.g. Bergantini, Zhu & Kaiser 2018b), we have compiled a comprehensive index of N–O bearing molecules with general formula $C_xN_yO_z$ ($x \geq 0$) and nominal mass up to 120 Da. The data were collected from *PubChem's* data base (Kim et al. 2021) for analysis as potential candidates for reference in further computational, laboratory, or observational studies. A total of 58 theoretical isomeric species were found within these constraints (see Table SI-1, S*upplementary Information*). Among them, 43 are radicals, including some exotic and extremely unstable species, whose detection is improbable in such studies. Among the 15 charge-neutral species found, 7 are nitrogen oxides, 5 of which were detected in our experiment according to reference infrared bands (see Tables 1 and 2). Thus, there are potentially eight hydrogen-free, charge-neutral isomeric species containing both at least one carbon atom and one N–O bond, none of which was detected either in this study, in the study of de Barros et al. (2020), or in the interstellar medium so far. Clearly, without proper reference of their infrared bands, the possibility that any given isomer had been synthesized in laboratory cannot be completely excluded, but one may at least say that there are no obvious signs of their presence as well.

5 CONCLUSIONS

Interstellar nitrogen-chemistry is extremely complicated in comparison with the chemistry of carbon and oxygen. In fact, Langer and Graedel (1989) have even called it 'vexing'. Astrochemical models of simple N-bearing molecules must account for the (high) ionization potential of nitrogen of 14.5 eV, which is beyond the Lyman limit. Therefore, cosmic-ray-induced chemistry must be considered. According to Langer & Graedel (1989), in the gas phase, unless N^+ can react efficiently with H_2, it will not enter the molecular cycle (e.g. $N^+ \; H_2 \; NH^+ \; H$). Alternatively, reactions of radicals with N are sufficient to initiate molecule production and convert atomic nitrogen into molecules in many cases (e.g. $CH_3^+ + N \rightarrow HCN^+ + H_2$). However, even in mechanisms in which larger C_xN_y species are involved, the reaction with astrophysically important oxygen bearing radicals, such as HCO^+ for example, rarely lead to NO bearing molecules (e.g.

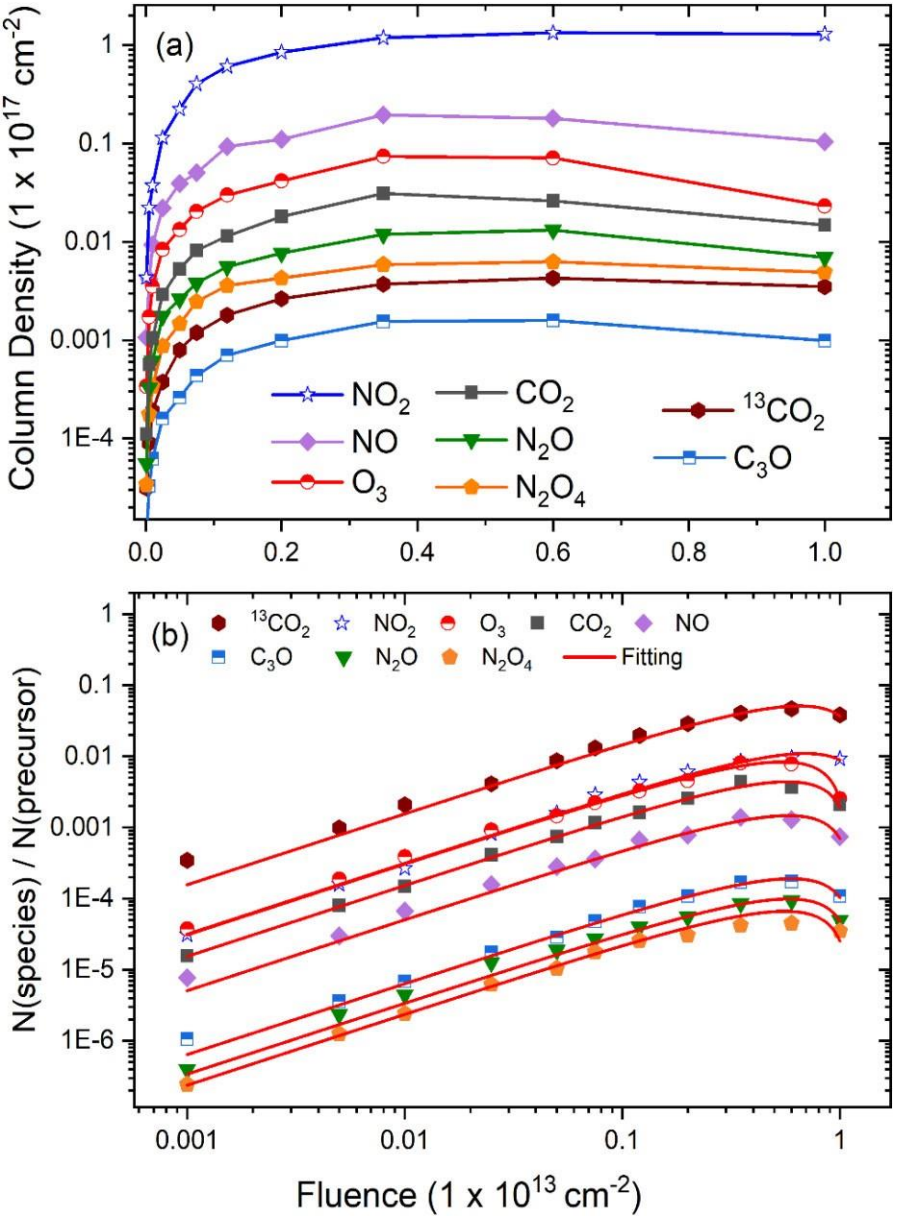

Figure 7. (a) Evolution of the column densities of products as a function of fluence. (b) Column density of each product normalized to $N_0(CO)$ and exhibited in log–log scale to stress the linear dependence on F at low fluences. Solid curves (red) are fittings performed using equation (2).

HCO^+ $C_xN_yH_z$ $C_xN_yH_{z+1}$ CO); Herbst & Leung 1989). Therefore, computational models and laboratory data confirm that the interstellar nitrogen chemistry is dominated by reactions with hydrogen, rather than carbon or oxygen.

Albeit the aphorism '*the absence of evidence is not evidence of absence*' still generally holds, the results presented here and in our previous study (de Barros et al. 2020), aided by data from literature, show no evidence of formation of any CN–O species, or $N_{x>2}O_y$ species in astrophysically relevant, nitrogen-rich apolar ices. Consequently, we suggest that the synthesis of such species within in astrophysical objects is either lacking, or, at least, remarkably inefficient (enough to make its detection beyond reach so far) – a question that still requires support from additional experimental, computational, and observational data. In conclusion, even though the Cosmo-chemistry of simple molecules, such as HNO, HONO, NO, and N_2O, have been extensively studied (e.g. Ziurys et al. 1994; Jamieson et al. 2005; Congiu et al. 2012; Fedoseev et al. 2016; Coutens et al. 2019), the feasibility of the existence of larger N–O species in ISM objects is far from being certain. In fact, Jamieson et al. (2006) and Duarte et al. (2010) concluded that ozone and oxygen atoms did not play a significant role in the formation routes larger oxocarbons upon cosmic-ray processing of CO ices. Similarly, Ioppolo et al. (2014) and Minissale et al. (2014) discovered that no allotropes of oxygen were involved on the formation of larger N–O and N–O–H bearing species, such as $ONNO_2$ and NH_2OH, which were formed from hydrogen addition to NO. Therefore, a logic conclusion is that, upon radiolysis of the astrophysically relevant species discussed here and in our previous work (i.e. N_2, NO, CO, and NH_3), the released oxygen atoms and ions will not be inducive of synthesizing larger nitrogen oxides ($N_{x>2}O_y$), nor larger species containing hydrogen, carbon, *and* an N-O bond, with few exceptions (e.g. hydroxylamine; Fedoseev et al. 2016). However, when other

Table 3. Parameters used in the calculation of the column densities of the products, as well as their formation (σ_f) and destruction (σ_d) cross-sections.

Species	Position (cm^{-1})	Band-strength (10^{-17} cm molecule^{-1})	σ_f (10^{-14} cm^2)	σ_d (10^{-13} cm^2)
Precursors				
CO	2139	1.1[a]	–	1.18
^{13}CO	2092	1.3[a]	–	1.03
Products				
CO_2	2347	7.6[a]	1.23	1.75
$^{13}CO_2$ [b]	2281	7.8[a]	1.52	1.52
C_3O	2263	19.0[c]	0.16	1.67
N_2O	2235	5.7[d]	0.09	1.72
NO	1875	0.45[e]	0.76	1.73
NO_2	1615	0.62[d]	1.35	1.44
N_2O_4	1262	8.5[f]	0.05	1.78
O_3	1042	1.4[c]	1.38	1.84

References: [a]Bouilloud et al. (2015); [b]The formation cross-section of $^{13}CO_2$ was calculated under the assumption that it was synthesized solely from ^{13}CO; [c]Jamieson et al. (2006); [d]Fulvio et al. (2009); [e]Sicilia et al. (2012); [f] Stirling et al. (1994).

mechanisms are considered, such as hydrogen addition, different results may be found (e.g. Minissale et al. 2014). Furthermore, the study of complementary, water-rich ice mixtures, in the same line of research as the work presented here, is extremely important for a better understanding of these phenomena and should be carried soon.

Finally, it is worth mentioning that our results are in good agreement with published studies, most notably, the results of Sicilia and colleagues on a similar system (Sicilia et al. 2012). Both studies found a series of similar unknown infrared bands (see Tables 1 and 2), which must be carefully investigated in the future. It is also worth mentioning the effects of signal processing methods, such as LOWESS, S-G filtering, and peak fitting, in extracting additional information from spectroscopic data, as demonstrated here and in our previous study (de Barros et al. 2020).

SUPPORTING INFORMATION

Table SI-1. Theoretical CxNyOz (x 0; y 1; z 1) isomers that also contain an N-O bond, with monoisotopic mass up to 120 Da.

Figure SI-1. Infrared spectrum of the 2075-1900 cm-1 region.

ACKNOWLEDGEMENTS

The authors acknowledge the Instituto Serrapilheira, the French-Brazilian exchange program CAPES-COFECUB, CNPq (INEspaço), FAPERJ, and CAPES. AB received financial support from Instituto Serrapilheira (Serra 1912–31853) and CNPq (Bolsa de Produtividade 303420/2019–7). ALFdeB received financial support from CNPq (Bolsa de Produtividade 301868/2017– 4, Projeto Universal 407938/2018–4), FINEP (0647/18), FAPERJ (Cientista do Nosso Estado E-245307/19, FAPERJ E-241202/18 and E-26/203.204/2017). This study was financed in part by the Coordenação de Aperfeiçoamento de Pessoal de Nível Superior – Brazil (CAPES) – Finance Code 001. We are grateful to the staff of GANIL and CIMAP, and in particular to T. Been, C. Grygiel, and J. M. Ramillon for their invaluable assistance during the experiments.

DATA AVAILABILITY

The data underlying this article will be shared on reasonable request to the corresponding author.

REFERENCES

Bassan P. et al., 2010, Analyst, 135, 268
Bennett C.J., Jamieson C.S., Kaiser R.I., 2009, PCCP, 11, 4210
Bennett C.J., Jamieson C.S., Mebel A.M., Kaiser R.I., 2004, PCCP, 6, 735
Bergantini A., Góbi S., Abplanalp M.J., Kaiser R.I., 2018a, ApJ, 852, 70
Bergantini A., Maksyutenko P., Kaiser R.I., 2017, ApJ, 841, 1
Bergantini A., Zhu C., Kaiser R.I., 2018b, ApJ, 862, 140
Bernstein M.P., Sandford S.A., 1999, AcSpA, 55, 2455
Blagojevic V., Petrie S., Bohme D.K., 2003, MNRAS, 339, L7
Bouilloud M., Fray N., Bénilan Y., Cottin H., Gazeau M.-C., Jolly A., 2015, MNRAS, 451, 2145
Bromba M.U., Ziegler H., 1981, AnaCh, 53, 1583
Cameron A.G., 1973, Space Sci. Rev., 15, 121
Charnley S., Rodgers S., Ehrenfreund P., 2001, A&A, 378, 1024
Ciaravella A., Jiménez-Escobar A., Cecchi-Pestellini C., Huang C., Sie N., Caro G.M., Chen Y., 2019, ApJ, 879, 21
Cleveland W.S., 1979, J. Am. Statist. Assoc., 74, 829
Congiu E., Chaabouni H., Laffon C., Parent P., Baouche S., Dulieu F., 2012, JChPh, 137, 054713
Coutens A. et al., 2019, A&A, 623, L13
de Barros A.L.F., Bergantini A., Domaracka A., Rothard H., Boduch P., da Silveira E.F., 2020, MNRAS, 499, 2162
de Barros A.L.F., Bordalo V.S.D.E., Duarte E.S., da Silveira E.F., Domaracka A., Rothard H., Boduch P., 2011, A&A, 531, A160
de Barros A.L.F., da Silveira E.F., Bergantini A., Rothard H., Boduch P., 2015, ApJ, 810, 156
Duarte E.S., Boduch P., Rothard H., Been T., Dartois E., Farenzena L., Da Silveira E., 2009, A&A, 502, 599
Duarte E.S., de Barros A.L.F., da Silveira E.F., Domaracka A., Boduch P., Rothard H., 2021, MNRAS, 508, 4297
Duarte E.S., Domaracka A., Boduch P., Rothard H., Dartois E., da Silveira E.F., 2010, A&A, 512, A71
Fateley W.G., Bent H.A., Crawford B., Jr. 1959, JChPh, 31, 204
Fedoseev G., Chuang K.-J., van Dishoeck E.F., Ioppolo S., Linnartz H., 2016, MNRAS, 460, 4297
Fedoseev G., Ioppolo S., Lamberts T., Zhen J., Cuppen H.M., Linnartz H., 2012, JChPh, 137, 054714
Fulvio D. et al., 2019, MNRAS, 483, 381
Fulvio D., Sivaraman B., Baratta G., Palumbo M., Mason N., 2009, AcSpA, 72, 1007
Herbst E., Leung C.M., 1989, ApJS, 69, 271
Hudson R.L., 2018, ApJ, 867, 160
Ioppolo S., Fedoseev G., Minissale M., Congiu E., Dulieu F., Linnartz H., 2014, Phys. Chem. Chem. Phys., 16, 8270
Jamieson C.S., Bennett C.J., Mebel A.M., Kaiser R.I., 2005, ApJ, 624, 436
Jamieson C.S., Kaiser R.I., 2007, Chem. Phys. Lett., 440, 98
Jamieson C.S., Mebel A.M., Kaiser R.I., 2006, ApJS, 163, 184
Kim S. et al., 2021, Nucleic. Acids. Res., 49, D1388
Krim L., 1998, J. Mol. Struct., 471, 267
Langer W.D., Graedel T., 1989, ApJS, 69, 241
Liszt H., Turner B., 1978, ApJS, 224, L73
McGonagle D., 1995, Doctor of Philosophy, University of Massachusetts Amherst
Mej´ıa C.F., de Barros A.L.F., Bordalo V., da Silveira E.F., Boduch P., Domaracka A., Rothard H., 2013, MNRAS, 433, 2368
Meyer D.M., Jura M., Cardelli J.A., 1998, ApJ, 493, 222
Miljkovic´ M., Bird B., Diem M., 2012, Analyst, 137, 3954

Minissale M., Fedoseev G., Congiu E., Ioppolo S., Dulieu F., Linnartz H., 2014, Phys. Chem. Chem. Phys., 16, 8257
Müller H.S., Thorwirth S., Roth D., Winnewisser G., 2001, A&A, 370, L49
Ponciano C., Martinez R., Farenzena L., Iza P., Homem M., Naves de Brito A., Wien K., Da Silveira E., 2008, J. Mass Spectrom., 43, 1521
Pulliam R.L., McGuire B.A., Remijan A.J., 2012, ApJ, 751, 1
Rivilla V.M. et al., 2020, ApJ, 899, L28
Sakurai M., Yanagawa H., 1984, Orig. Life, 14, 171
Sicilia D., Ioppolo S., Vindigni T., Baratta G., Palumbo M.E., 2012, A&A, 543, A155
Socrates G., 1994, Infrared and Raman Characteristic Group Frequencies: Tables and Charts. 2nd Ed., J. Wiley & Sons, Chichester
Stirling A., Pápai I., Mink J., Salahub D.R., 1994, JChPh, 100, 2910
Tian R., Facelli J.C., Michl J., 1988, JPhCh, 92, 4073
Varetti E.L., Pimentel G.C., 1971, JChPh, 55, 3813
Ziegler J.F., Ziegler M.D., Biersack J.P., 2010, Nucl. Instrum. Methods. Phys. Res. Sect. B., 268, 1818
Ziurys L.M., Apponi A., Hollis J., Snyder L., 1994, ApJ, 436, L181